Regrowth-related defect formation and evolution in 1 MeV amorphized (001) Ge

D. P. Hickey,[a] Z. L. Bryan, and K. S. Jones
SWAMP Center, University of Florida, 525 New Engineering Bldg., PO Box 116130, Gainesville, FL 32611-6130

R. G. Elliman
Electronic Materials Engineering Department, Research School of Physical Sciences and Engineering, The Australian National University, Canberra ACT 0200, Australia

E. E. Haller
Materials Sciences Division, Lawrence Berkeley National Laboratory and Department of Materials Science and Engineering, University of California at Berkeley, Mail Code 1760, 328 Hearst Memorial Mining Building, Berkeley, CA 94720-1760

(Received 8 January 2007; accepted 23 February 2007; published online 28 March 2007)

Ge implanted with 1 MeV Si^+ at a dose of 1×10^{15} cm^{-2} creates a buried amorphous layer that, upon regrowth, exhibits several forms of defects–end-of-range (EOR), regrowth-related, and clamshell defects. Unlike Si, no planar {311} defects are observed. The minimal EOR defects are small dotlike defects and are very unstable, dissolving between 450 and 550 °C. This is in contrast to Si, where the EOR defects are very stable. The amorphous layer results in both regrowth-related defects and clamshell defects, which were more stable than the EOR damage. © *2007 American Institute of Physics*. [DOI: 10.1063/1.2717538]

Interest in germanium (Ge) has been growing in recent years. Ge has higher carrier mobilities than silicon (Si) (3800 vs 1900 cm^2/V s for electrons and 1820 vs 500 cm^2/V s for holes),[1] making it attractive for a channel material. Many studies have investigated the electrical aspects of implanting dopants into Ge.[2,3] This has been facilitated by the possible introduction of high-*k* dielectrics which would circumvent the problems associated with the unstable gate oxide. In addition, SiGe alloys are being used in the current generation of devices to induce strain in the transistor channel.[4] Ion implantation is often used in doping the SiGe prior to silicidation.[5] Despite the renewed interest in Ge, relatively little knowledge of the formation and evolution of ion-implantation-related defects in Ge exists.

In Si, amorphization results in end-of-range (EOR) defects that are initially observed as planar {311} defects and evolve into stable dislocation loops upon annealing.[6] End-of-range defects can dominate dopant diffusion and leakage in junctions formed using amorphizing implants. In addition, a buried amorphous layer has been shown to produce regrowth-related defects as well as clamshell defects in Si.[7]

Recent transmission electron microscopy (TEM) studies of dopant implants into Ge reported no EOR damage formation for amorphizing implants.[2,8–11] However, these were lower-energy implants and the EOR defect density is known to increase with increasing implant energy.[12] Extended defects in Ge, reported as {311} defects, have been observed after nonamorphizing light ion implantation[13] and electron irradiation.[14] No published reports exist on the formation of stable regrowth related-defects or clamshell defects in implanted Ge. The purpose of this study is to understand the defect formation and evolution from a high-energy implant of Si ions into Ge that produces a buried amorphous layer.

Undoped (001) Czochralski grown high-purity Ge wafers were implanted in a tandem accelerator with 1 MeV Si^+ ions at 30 °C to a dose of 1×10^{15} cm^{-2} with 7° of tilt. The wafers were capped with 1000 Å SiO_2 via plasma-enhanced chemical vapor deposition at 300 °C for 3 min to prevent possible oxidation during furnace annealing. Subsequent annealing was conducted for 10 min in a N_2 ambient at temperatures between 350 and 850 °C in a Lindberg tube furnace. Solid phase epitaxial recrystallization of ion-implantation induced amorphous layers in Ge is known to occur at approximately 400 °C.[15,16] After annealing, cross-section TEM samples (XTEM) were prepared using an FEI dual beam focused ion beam and Omniprobe lift-out system. Transmission electron microscopy analysis was performed on a JEOL 200CX using g_{220} weak beam dark field (WBDF) imaging conditions and a JEOL 2010 for high-resolution imaging.

The implant conditions created a buried amorphous layer starting approximately 0.1 μm below the surface and extending to a depth of 1.2 μm as shown in Fig. 1(a). The WBDF images show that both the upper and lower amorphous-crystalline (α-*c*) interfaces are rough. This agrees well with the rough α-*c* Ge interface previously reported after an amorphizing implant.[8,11] Transmission electron microscopy analysis shows that the near surface region is not completely crystalline but rather contains pockets of crystalline material embedded in the amorphous Ge [Fig. 2(a)]. High-resolution TEM lattice imaging confirmed the crystalline nature of the pockets of embedded Ge in the near surface region. Transmission electron microscopy of the as-implanted lower α-*c* interface also shows pockets of crystalline Ge embedded in the amorphous phase along the rough interface region, shown in Fig. 2(b). The transition region for the upper interface is approximately 140 nm, while the lower interface is much more abrupt at 65 nm. By comparing the depths of the amorphous layer with TRIM (Ref. 17) calculations of the im-

[a]Electronic mail: dhickey@ufl.edu

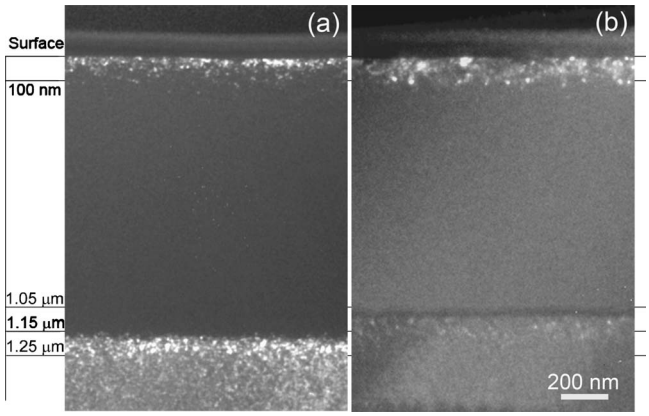

FIG. 1. WBDF XTEM images taken at g_{220} diffraction conditions of (001) oriented Ge implanted with 1 MeV, 1×10^{15} Si^{+} cm^{-2} (a) after implantation and (b) 10 min at 350 °C.

plant, assuming a displacement energy of 15 eV, the threshold damage density (TDD) for amorphization of Ge by a room temperature implant was estimated to be in the range of 3.7×10^{20} to 4.2×10^{20} keV cm^{-3}. For 500 keV Si^{+} implants at 77 K, the surface TDD of Ge is approximately 2.5×10^{20} keV cm^{-3}.[18] The lower TDD at 77 K is expected because of reduced dynamic annealing. Si has a reported surface TDD for P implantation of 1.0×10^{21} keV cm^{-3}.[19] The EOR amorphization threshold follows the same trends. This suggests that it is easier to amorphize Ge than Si which is consistent with Ge's lower melting point.

After annealing the sample at 350 °C for 10 min, approximately 100 nm of regrowth was observed, as shown in Fig. 1(b). This agrees well with the reported 350 °C regrowth rate in the (001) Ge of 9 nm/min of Csepregi *et al.*[15] This regrowth created a significantly smoother α-c interface. End-of-range damage is observed after 10 min at 350 °C and consists of small dotlike defects that extend beyond the α-c interface. End-of-range dislocations in implanted Ge have not been previously reported. After annealing at 350 °C for 10 min, planarization of the bulk interface occurred, while no well-defined crystalline advancing front developed in the near-surface region. Figure 3(a) shows that after annealing at 450 °C, the Ge has completely recrystallized. Regrowth-related defects, clamshell (or zipper) defects, and EOR defects are observed. Regrowth-related defects, which appear as threading dislocations with a primarily vertical line direction in the image, are the result of imperfect solid phase epitaxial recrystallization. These defects are known to nucleate at either a rough interface or when the solid phase epitaxial growth process proceeds around an embedded crystalline region.[20] The density of regrowth-related defects appears greater in the layer that nucleated at the surface. This may be the result of the wider transition region near the surface.

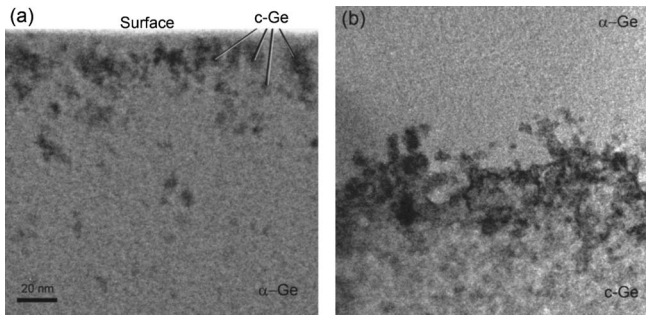

FIG. 2. HRTEM images taken on axis of (001) oriented Ge implanted with 1 MeV, 1×10^{15} Si^{+} cm^{-2} as implanted: (a) surface crystalline-to-amorphous transition region and (b) end-of-range amorphous-to-crystalline transition region.

Clamshell defects occur when the two advancing crystalline growth planes meet and are approximately parallel to the surface.[7] Previous studies have suggested that these defects in Si have a Burgers vector parallel to the surface and thus have a pure shear character. Transmission electron microscope $g\cdot b$ analysis using many two-beam conditions indicate that these dislocations in Ge do not display the shear nature. Instead the dislocation appears to be a mixture of 60° and 90° dislocations. The EOR defects are approximately 1.1 μm below the surface and appear to be loops similar to what is seen in Si.[7] These dislocation loops appear to evolve from small loops. No {311} defects are ever observed in the defect evolution process. This suggests that, unlike in Si where it has been shown that {311} defects unfault into dislocation loops, in Ge the loops appear to skip this step and evolve directly from submicroscopic clusters to dislocation loops.[6] If {311} defects do form in the EOR region and unfault into loops, the defects must do this before becoming visible in WBDF imaging conditions.

Regrowth-related damage is still apparent after 10 min at 550 °C, as shown in Fig. 3(b), though a reduction in EOR damage density occurred from the 450 °C anneal, indicating that the EOR defects are relatively unstable in Ge. After the 650 °C anneal, no EOR and virtually no clamshell defects remain [Fig. 3(c)]. Only the regrowth-related defects are still visible in the TEM image. Therefore, it can be concluded that regrowth-related defects are the most stable in high-energy implants into Ge. Very few regrowth-related defects remain after anneals at 750 °C [Fig. 3(d)], and at 850 °C (not shown) no defects remain (defect density $<10^{8}$ cm^{-2}).

The type and stability of defects found in this study differ from what have been previously reported for Si defects. Unlike Si, few EOR defects were observed during the Ge regrowth process. The existing Ge EOR defects were the initial defects to dissolve between 450 and 550 °C. The clamshell or zipper defects annealed out between 550 and 650 °C. The regrowth-related defects, also known as hairpin dislocations, were clearly visible after 10 min at 450 °C and did not dissolve below 750 °C. The regrowth-related defects lack the morphology of the hairpin dislocation seen in Si.[20] The line direction of the regrowth defects in Si is observed to be very similar to what is observed in these samples. In Ge, the line direction appears to move but this may be related to the increased density of dislocation in the upper regrowth layer. A $g\cdot b$ analysis of the Ge regrowth defects confirmed that the Burgers vectors are perfect with $\vec{\mathbf{b}}=(a/2)\langle110\rangle$. Jones *et al.* reported that in Si, hairpin dislocations were less stable than clamshell defects, which were in turn less stable than EOR defects.[7] In Si, EOR defects are the most stable defect, while we find that in Ge, EOR defects are the least stable of the three types of defects. It has been shown in Si that reducing the TDD for amorphization either by increasing the implant temperature or increasing the dose rate results in fewer EOR defects.[12] The decrease in EOR defect density and stability in Ge, as compared to Si, may be results of fewer interstitials in the EOR available to form extended defects. As previously noted, the TDD in Ge is less than in Si, making it easier to amorphize Ge than Si using the same

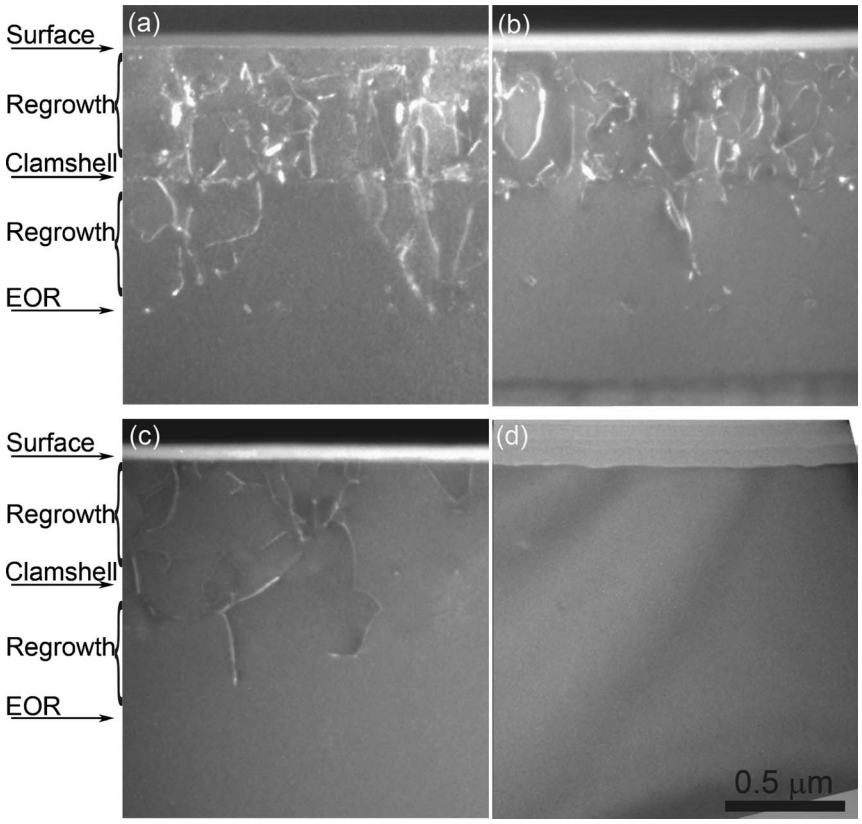

FIG. 3. WBDF XTEM images taken at g_{220} diffraction conditions of (001) oriented Ge implanted with 1 MeV, 1×10^{15} Si^{+} cm^{-2} anneal for 10 min at (a) 450 °C, (b) 550 °C, (c) 650 °C, and (d) 750 °C. Types of defects are labeled next to the images.

implant. Therefore, for the same damage profile, more of the total damage profile is within the amorphous range for Ge, leaving less interstitials in the EOR region available for defect formation.

In summary, TEM was used to characterize the extended defects arising from annealing implantation induced amorphized Ge. Although {311} defects have been previously reported in Ge after light ion implantation[13] and electron irradiation,[14] in this study, no {311} defects were observed over a wide range of annealing temperatures. EOR dislocation loops were observed, possibly due to the high implant energy, as these defects have not been seen in previous lower-energy studies.[2,8–11] In addition, regrowth-related defects and clamshell defects were also observed, with regrowth-related defects exhibiting the greatest stability.

This work is supported by Semiconductor Research Corporation Contract No. 00057787. All instrumentation used in this study is located at the University of Florida's Major Analytical Instrumentation Center. D.P.H. would like to thank N. G. Rudawski for useful discussions pertaining to the $g\cdot b$ analysis.

[1]L. L. Berger, *in CRC Handbook of Chemistry and Physics*, edited by David R. Lide (Taylor & Francis, London, 2005), pp. 12–82.
[2]Y. L. Chao, S. Prussin, J. C. S. Woo, and R. Scholz, Appl. Phys. Lett. **87**, 142102 (2005).
[3]Yong Seok Suh, Malcolm S. Carroll, Roland A. Levy, Gabriele Bisognin, D. De Salvador, M. Alper Sahiner, and Clifford A. King, IEEE Trans. Electron Devices **52**, 2416 (2005).
[4]P. R. Chidambaram, C. Bowen, S. Chakravarthi, C. Machala, and R. Wise, IEEE Trans. Electron Devices **53**, 944 (2006).
[5]Y. S. Li, P. S. Lee, and K. L. Pey, Thin Solid Films **462–463**, 209 (2004).
[6]J. H. Li and K. S. Jones, Appl. Phys. Lett. **73**, 3748 (1998).
[7]K. S. Jones, S. Prussin, and E. R. Weber, Appl. Phys. A: Mater. Sci. Process. **45**, 1 (1988).
[8]A. Satta, T. Janssens, T. Clarysse, E. Simoen, M. Meuris, A. Benedetti, I. Hoflijk, B. De Jaeger, C. Demeurisse, and W. Vandervorst, J. Vac. Sci. Technol. B **24**, 494 (2006).
[9]A. Satta, E. Simoen, R. Duffy, T. Janssens, T. Clarysse, A. Benedetti, M. Meuris, and W. Vandervorst, Appl. Phys. Lett. **88**, 162118 (2006).
[10]A. Satta, E. Simoen, T. Janssens, T. Clarysse, B. De Jaeger, A. Benedetti, I. Hoflijk, B. Brijs, M. Meuris, and W. Vandervorst, J. Electrochem. Soc. **153**, G229 (2006).
[11]A. Satta, E. Simoen, T. Clarysse, T. Janssens, A. Benedetti, B. De Jaeger, M. Meuris, and W. Vandervorst, Appl. Phys. Lett. **87**, 172109 (2005).
[12]K. S. Jones and D. Venables, J. Appl. Phys. **69**, 2931 (1991).
[13]T. Akatsu, K. K. Bourdelle, C. Richtarch, B. Faure, and F. Letertre, Appl. Phys. Lett. **86**, 181910 (2005).
[14]C. A. Ferreira Lima and A. Howie, Philos. Mag. **34**, 1054 (1976); I. G. Salisbury and M. H. Loretto, Philos. Mag. A **39**, 317 (1979); M. Pasemann, D. Hoehl, A. L. Aseev, and O. P. Pchelyakov, Phys. Status Solidi A **80**, 135 (1983); H. Bartsch, D. Hoehl, and G. Kastner, *ibid.* **83**, 543 (1984); S. Furuno, K. Izui, and H. Otsu, Jpn. J. Appl. Phys. **15**, 889 (1976).
[15]L. Csepregi, R. P. Kullen, J. W. Mayer, and T. W. Sigmon, Solid State Commun. **21**, 1019 (1977).
[16]K. Zellama, J. F. Morhange, P. Germain, and J. C. Bourgoin, Phys. Status Solidi A **56**, 717 (1979).
[17]J. F. Ziegler, Nucl. Instrum. Methods Phys. Res. B **219–220**, 1027 (2004).
[18]R. Elliman (private communication).
[19]S. Prussin, D. I. Margolese, and R. N. Tauber, J. Appl. Phys. **57**, 180 (1985).
[20]T. Sands, J. Washburn, R. Gronsky, W. Maszara, D. K. Sadana, and G. A. Rozgonyi, 13th International Conference on Defects in Semiconductors, Coronado, CA, 1984 (unpublished), pp. 531–537.